

Supporting Information

Sustainable and affordable composites built using microstructures performing better than nanostructures for arsenic removal

*Sritama Mukherjee[†], Avula Anil Kumar[†], Chennu Sudhakar[†], Ramesh Kumar[†], Tripti Ahuja[†],
Biswajit Mondal[†], Srikrishnarka Pillalamarri[†], Ligy Philip[‡], Thalappil Pradeep^{*, †}*

[†] DST Unit of Nanoscience (DST UNS) and Thematic Unit of Excellence (TUE), Department of Chemistry, Indian Institute of Technology Madras, Chennai 600036, India.

[‡] EWRE Division, Department of Civil Engineering, Indian Institute of Technology Madras, Chennai 600036, India.

*Corresponding author

E-mail: pradeep@iitm.ac.in

Thalappil Pradeep, DST Unit of Nanoscience (DST UNS) and Thematic Unit of Excellence (TUE), Department of Chemistry, Indian Institute of Technology Madras, Chennai 600036, India.

Tel.: +91-44 2257 4208; Fax: +91-44 2257 0545/0509

SUPPORTING INFORMATION CONTENT

Total number of pages: 18

Total number of figures: 12

Total number of tables: 1

Total number of equations: 8

TABLE OF CONTENTS

Supporting items	Title	Page no.
	Instrumentation	S3
E1-E8	Equations used in main text	S4-S5
Figure S1	SEM images of Cellulose nanocrystals	S6
Figure S2	Plot of horizontal shear stress vs. horizontal displacement of CMCFH	S7
Figure S3	Mohr-Coulomb failure pattern (Shear stress vs. Normal stress) of CMCFH	S8
Figure S4	HRTEM and EDS of CMCFH after As(III) and As(V) adsorption	S9
Figure S5	XRD of CMCFH annealed up to 900 °C	S10
Figure S6	IR spectra of CMCFH before and after As(III)/As(V) adsorption, corresponding to IR of As standards	S11
Figure S7	Pseudo first-order reaction kinetic plots for the adsorption of As(III) and As(V) on ferrihydrite	S12
Figure S8	Pseudo second-order reaction kinetic plots for the adsorption of As(III) and As(V) on ferrihydrite	S13
Figure S9	As (III) adsorption on MCCFH (a) Freundlich and (b) Dubinin–Radushkevich isotherm models	S14
Figure S10	Interfering ions (cations and anions) studies for (A) MCCFH, (B) CPFH and (C) HECFH, respectively	S15
Figure S11	SEM-EDS and elemental mapping of CMCFH before and after As(III)/As(V) adsorption	S16
Figure S12	Thermogravimetric analysis (TGA) of CMCFH at air and nitrogen atmospheres	S17
Table S1	Physicochemical characteristics of influent natural drinking water	S18

INSTRUMENTATION

Transmission electron microscopy (TEM) and high-resolution transmission electron microscopy (HRTEM) were performed at an accelerating voltage of 200 kV on a JEOL 3010, 300 kV instrument equipped with a UHR polepiece. The accelerating voltage was kept low to ensure that beam induced damage on the material was low. The samples for HRTEM were prepared as the dispersions which were dropcasted on carbon-coated copper grids and allowed to dry under ambient conditions. Surface morphology, elemental analysis and elemental mapping studies were carried out using a Scanning Electron Microscope (SEM) equipped with energy dispersive spectroscopy (EDS) (FEI Quanta 200). For the SEM and EDS measurements, the samples were spotted on an aluminum sample stub. X-ray Photoelectron Spectroscopy (XPS) measurements were done using an ESCA Probe TPD spectrometer of Omicron Nanotechnology. Polychromatic Mg K α was used as the X-ray source ($h\nu = 1253.6$ eV). Samples were spotted as drop cast films on a sample stub. Constant analyzer energy of 20 eV was used for the measurements. Binding energy was calibrated with respect to C 1s at 284.8 eV. Raman spectroscopy was performed using a CRM 200 micro Raman spectrometer of WiTec GmbH (Germany). The substrate was mounted on a sample stage of a confocal Raman spectrometer. The spectra were collected at 633 nm laser excitation. For Raman measurements, the corresponding nanomaterial/standard material (as in dried powder form)-coated glass substrates were analyzed keeping the laser and other parameters the same. Total As and iron concentrations in water were detected using PerkinElmer NexION 300X ICPMS (Inductively coupled plasma mass spectrometry) with appropriate standards. It is a type of mass spectrometry that is highly sensitive for analyzing a range of metal ions and capable of distinguishing their isotopic speciation. ICPMS detection systems use electron multipliers, which convert ion currents into electrical signals. The magnitude of the electrical signal is proportional to the number of analyte ions present in the sample. Brunauer–Emmett–Teller (BET) surface area was measured using Micromeritics ASAP 2020. Samples were degassed at 200 °C for 4 h under vacuum and analyzed at 77 K with ultrahigh pure nitrogen gas. Thermogravimetric measurement was done with TA Instruments Q500 Thermogravimetric Analyzer (TGA) under air and N₂ atmosphere from room temperature to 900 °C, with 10 min scan rate. All the uptake capacity studies in batch mode were done in 250 mL polypropylene conical flasks.

Equation (1): The maximum uptake of As (q_e) by cellulosic composites was calculated using the equation given below:

$$Uptake (qe) = \frac{(C_o - C_e)V}{m}$$

where q_e is the amount of As(III)/As(V) ions adsorbed per gram of the adsorbent (mg/g) at equilibrium, C_e is the equilibrium concentration of As(III)/As(V) in the bulk solution (mg/L), C_o is the initial As(III)/As(V) concentration (mg/L), V is the volume of solution (L) and m is the mass of the adsorbent (g).

Equation (2): The linearized form of Langmuir equation used in this work is defined as,

$$\frac{C_e}{q_e} = \frac{C_e}{q_{max}} + \frac{1}{bq_{max}}$$

where q_e is the amount of adsorption at the surface of the adsorbent (mg/g), C_e is the equilibrium concentration of the solution (mg/L), q_{max} is the maximum surface density at monolayer coverage and b is the Langmuir adsorption constant (L/mg) related to the free energy of adsorption and $1/q_{max}$ and $1/bq_{max}$ are the Langmuir constants.

Equation (3): The removal % of As was calculated using the equation mentioned below:

$$Removal \% = \frac{C_o - C_e}{C_o} \times 100$$

where C_o and C_e are the initial and equilibrium concentrations of the metal ions, respectively.

Sustainability metrics equations

Equation (4): $Mass\ intensity = \frac{mass\ of\ all\ products\ used\ excluding\ water}{mass\ of\ product} kg/kg\ product$

Equation (5): $Water\ intensity\ (W_p) = \frac{mass\ of\ all\ water\ used}{mass\ of\ product} kg/kg\ product$

Equation (6): Reaction mass efficiency (RME) = $\frac{\text{mass of product}}{\text{mass of all reactants}} \times 100\%$

Equation (7): *Energy Intensity* = $\frac{\text{amount of non renewable energy used}}{\text{mass of product}} \text{ kW.h/kg}$

Equation (8): *E factor* = $\frac{[\text{kg}(\text{raw materials}) - \text{kg}(\text{desired product})]}{\text{kg}(\text{total product including water})}$

Supporting Information 1

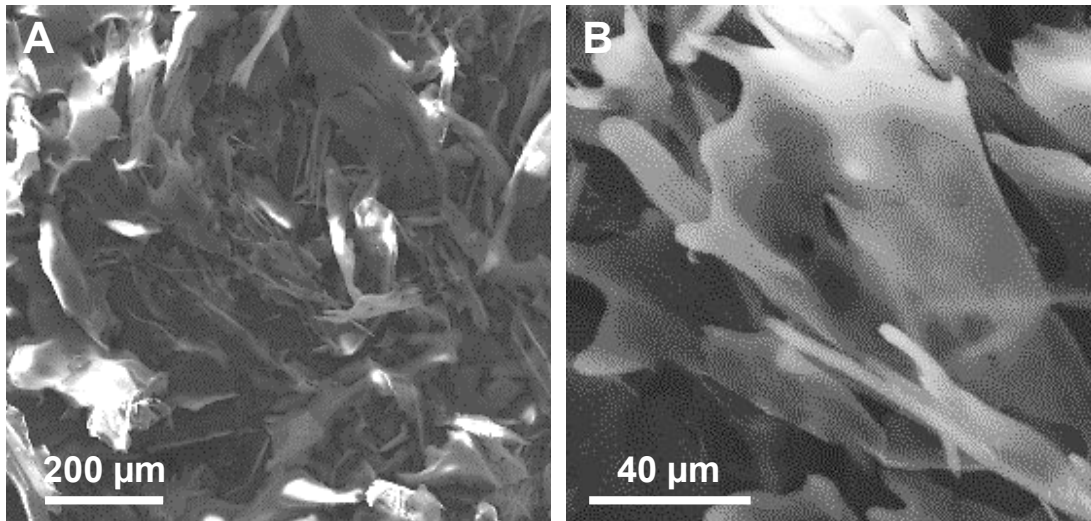


Figure S1. SEM images of cellulose nanocrystals at different length scales.

Supporting Information 2

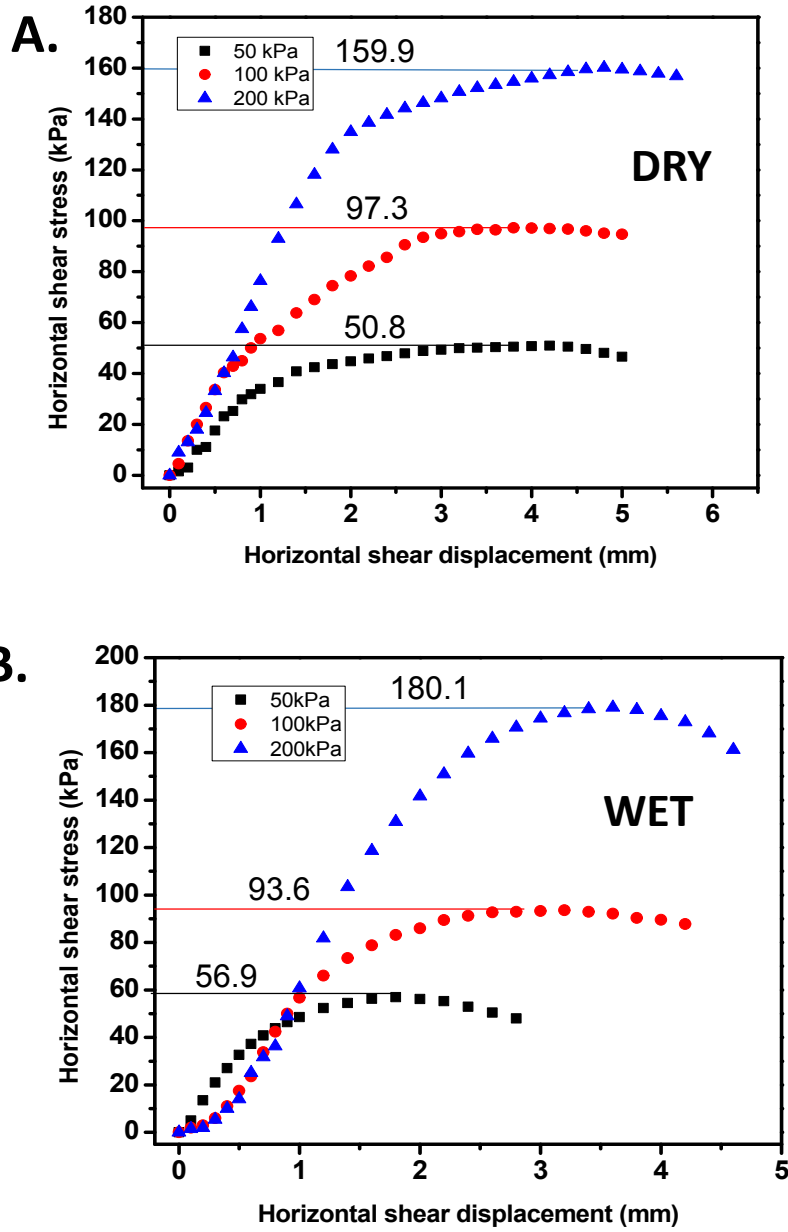


Figure S2. Direct shear test (Horizontal shear stress vs. Horizontal displacement). Plot of horizontal shear stress vs. horizontal displacement of loosely packed media obtained from direct shear tests: (A) measured at dry condition and (B) measured at wet condition.

Supporting Information 3

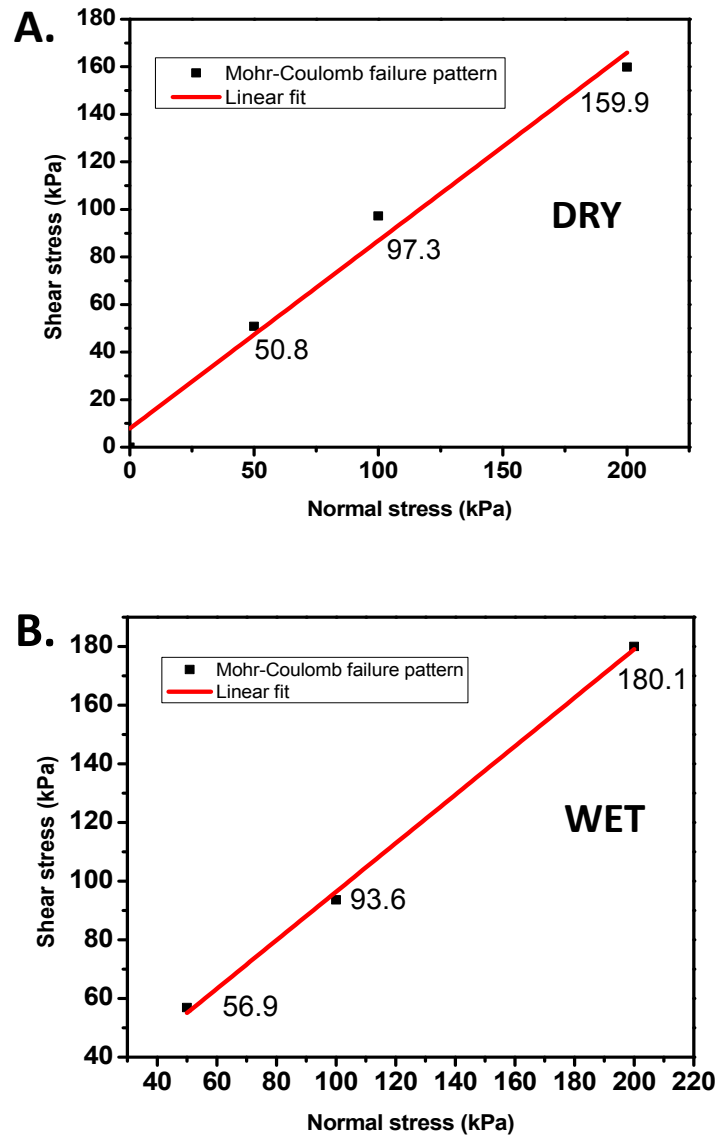


Figure S3. Mohr-Coulomb failure pattern (Shear stress vs. Normal stress). Plot of shear stress vs. normal stress of loosely packed media showing the straight-line approximation of the Mohr-Coulomb failure pattern: (A) measured at dry condition and (B) measured at wet condition.

Supporting Information 4

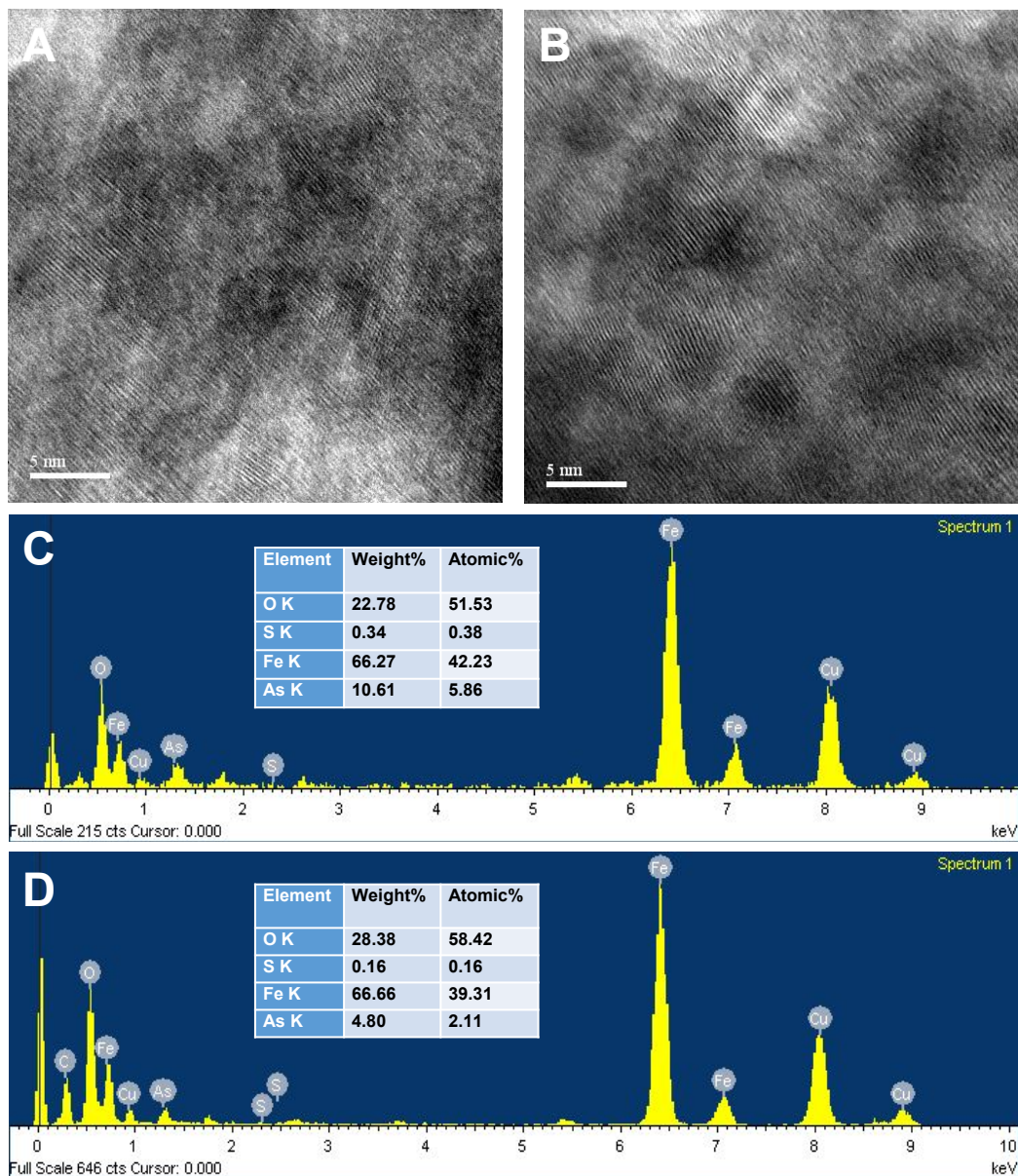


Figure S4. HRTEM and EDS of CMCFH after As(III) and As(V) adsorption. (A) and (B) show HRTEM micrograph of As(III) and As(V) adsorbed CMCFH, respectively, after beam induced crystallization. (C) and (D) show EDS of As(III) and As(V) adsorbed CMCFH, respectively.

Supporting Information 5

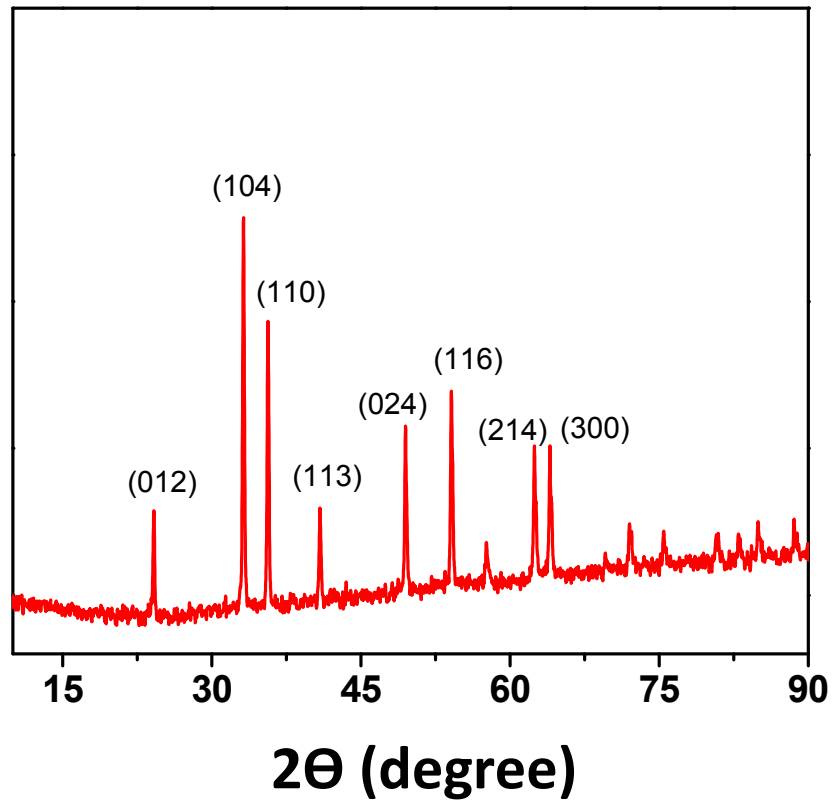


Figure S5. XRD of CMCFH annealed up to 900 °C showing hematite (α -Fe₂O₃) formation from ferrihydrite content of the composite.

Supporting Information 6

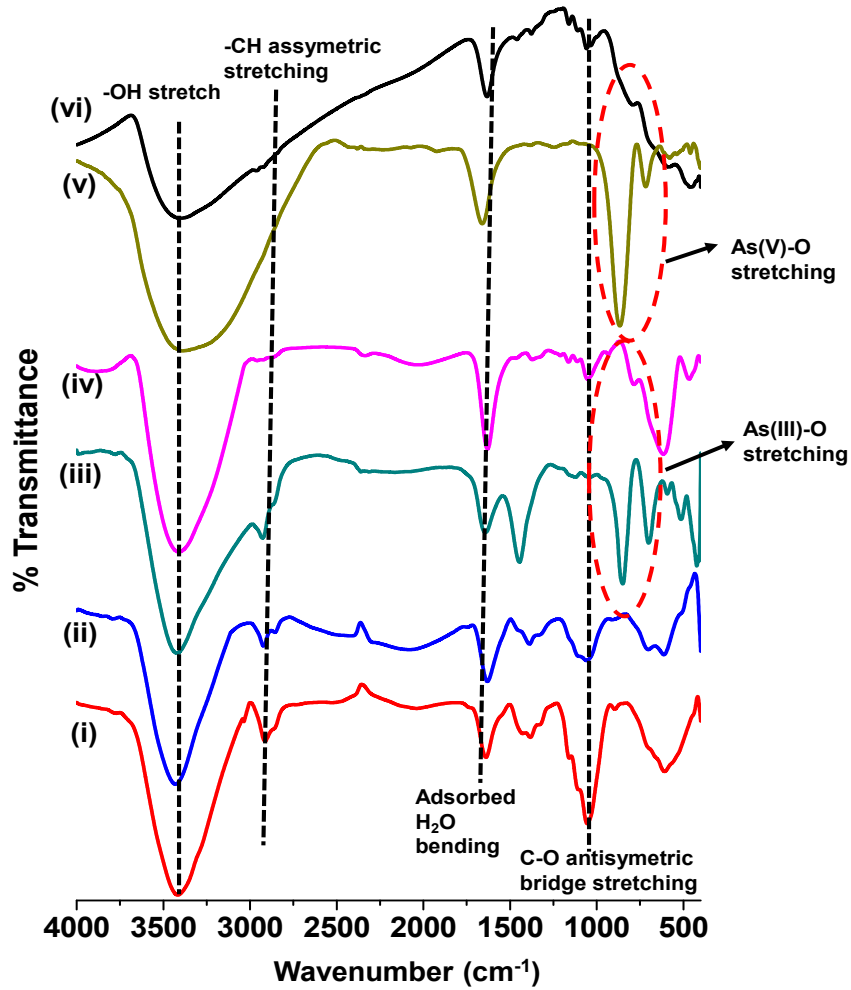


Figure S6. Infrared (IR) spectra of (i) cellulose; (ii) CMCFH solid; (iii) and (v) standard aqueous solutions of As(III) and As(V) at pH 7; (iv) and (vi) CMCFH before and after As(III) and As(V) adsorption, respectively.

Supporting Information 7

Lagergren pseudo-first-order model: $\ln(q_e - q_t) = \ln q_e - k_1 t$

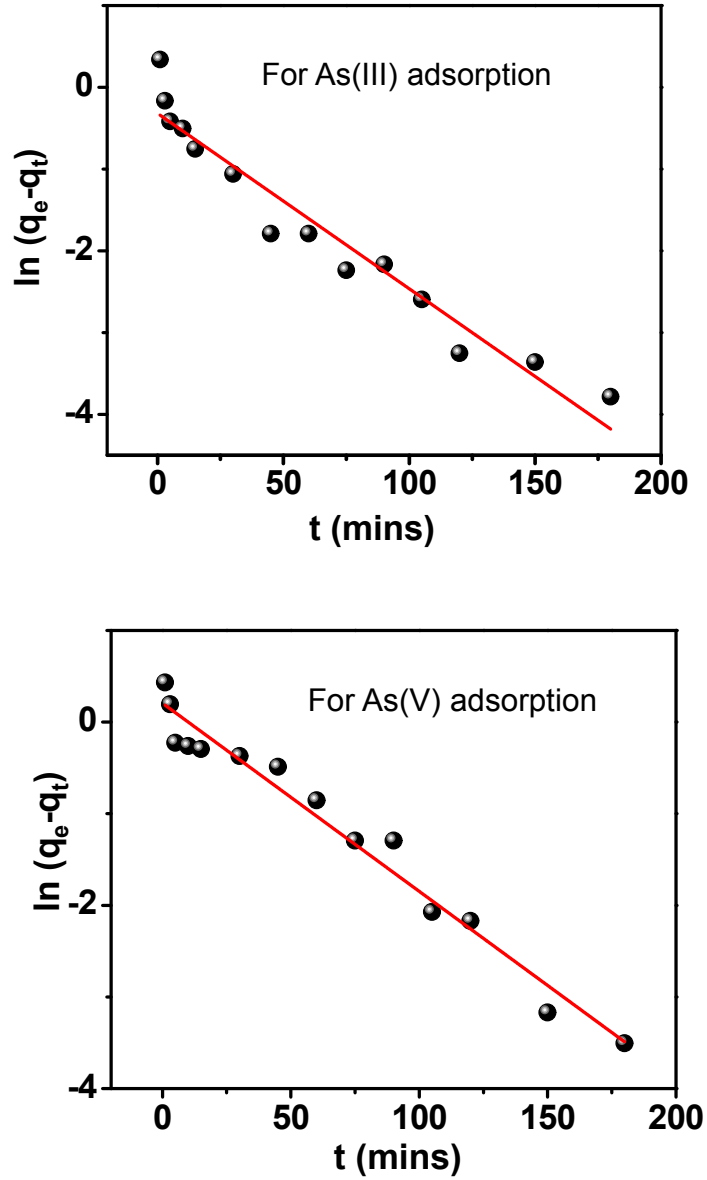


Figure S7. Pseudo first-order reaction kinetic plots for the adsorption of As(III) and As(V) on ferrihydrite.

Supporting Information 8

Ho's pseudo-second-order model: $\frac{t}{q} = \frac{1}{k_2 q_e^2} + \frac{1}{q_e} t$

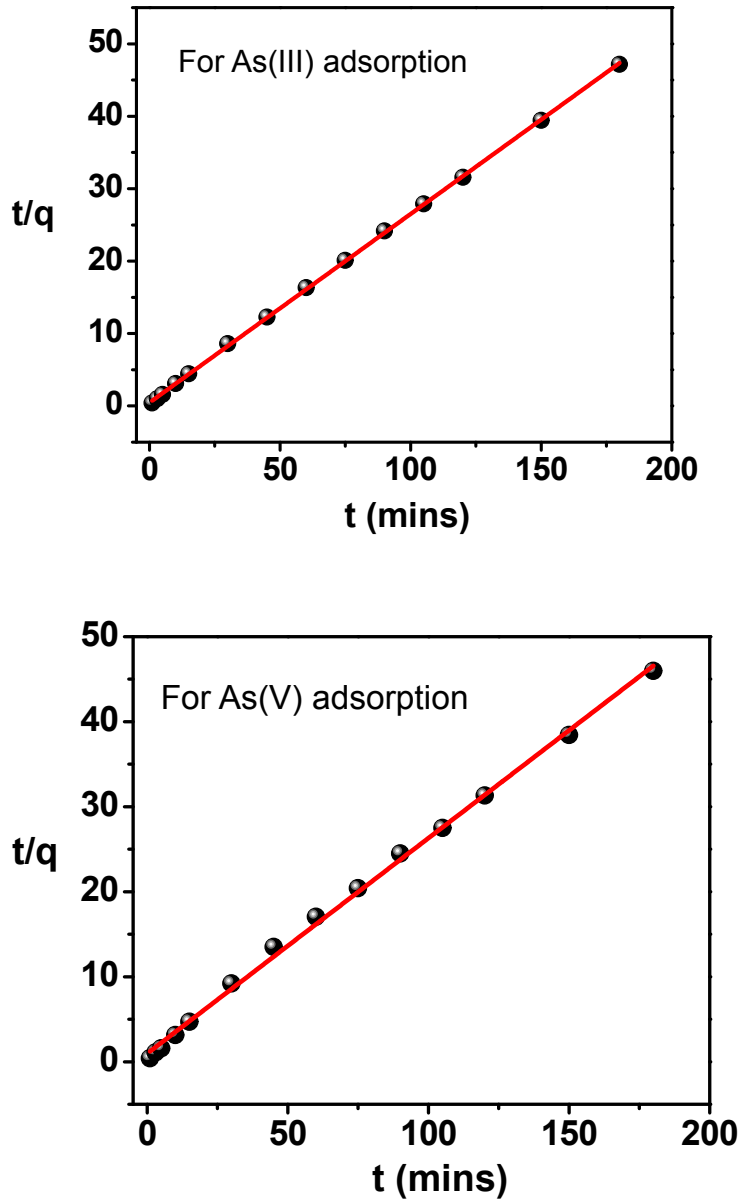
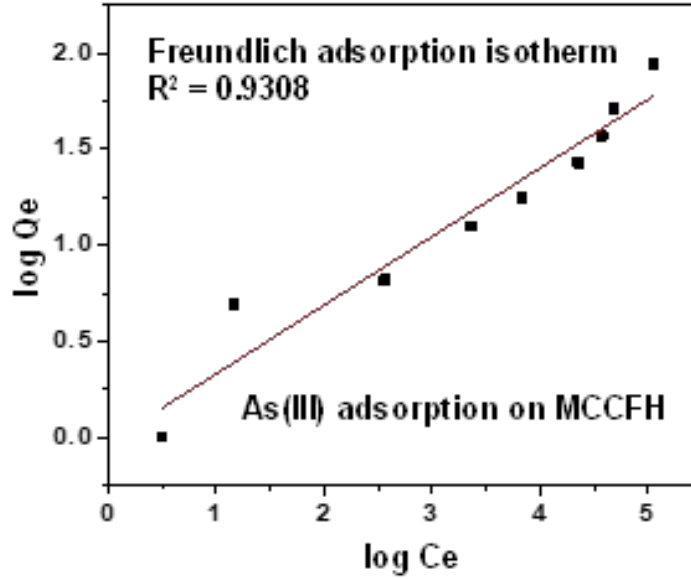


Figure S8. Pseudo second-order reaction kinetic plots for the adsorption of As(III) and As(V) on ferrihydrite.

Supporting Information 9

a. Freundlich adsorption isotherm model: $\log Q_e = \log K_f + \frac{1}{n} \log C_e$



b. Dubinin–Radushkevich isotherm model: $\ln Q_e = \ln Q_s - K_{ad} \varepsilon^2$

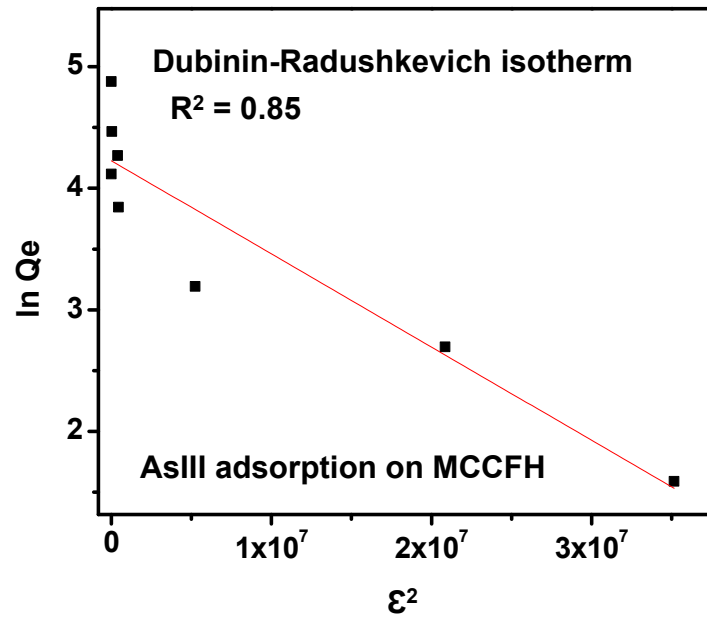


Figure S9. Adsorption isotherms showing the correlation coefficients for As (III) adsorption on MCCFH (a) Freundlich and (b) Dubinin–Radushkevich isotherm models, respectively.

Supporting Information 10

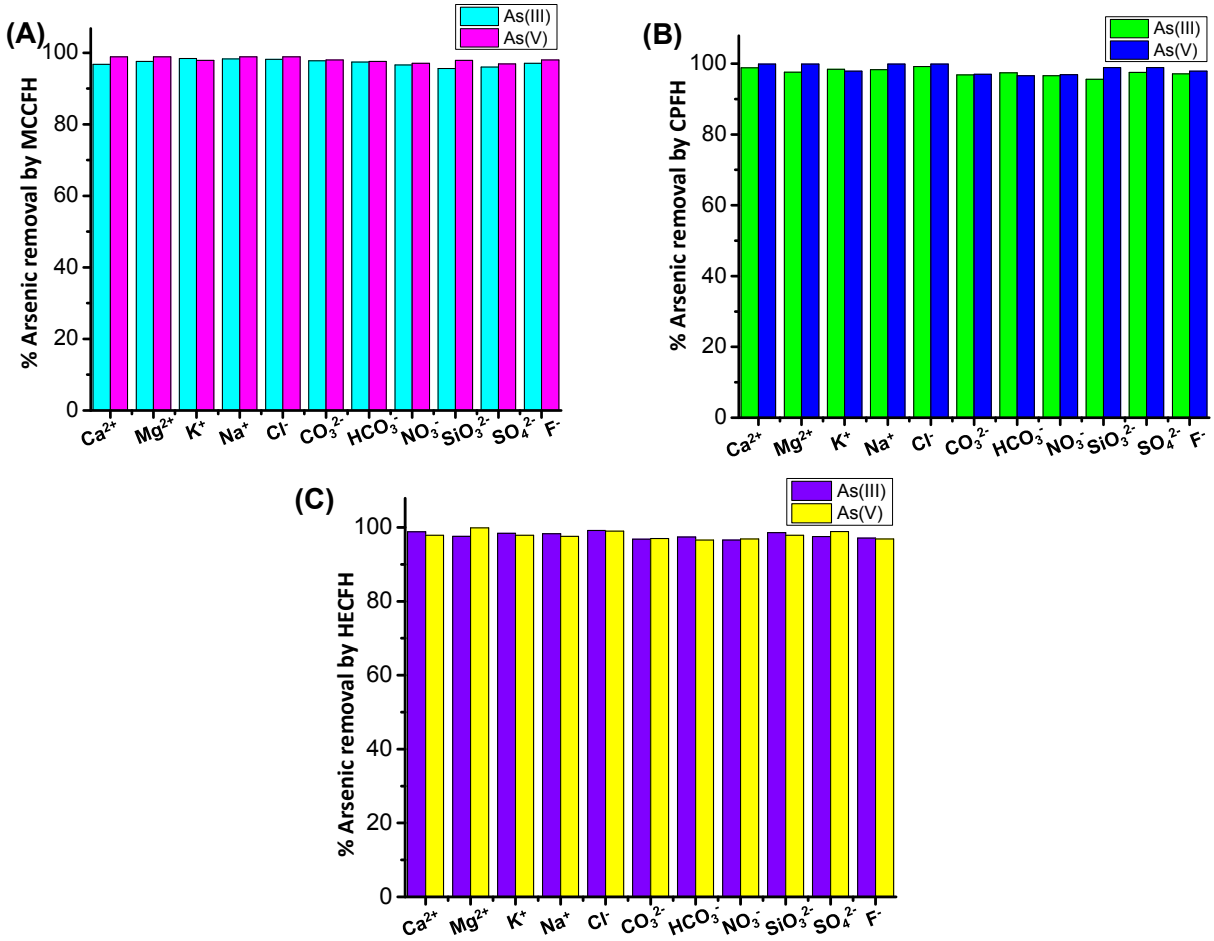


Figure S10. Uptake of As(III) and As(V) in presence of other competing ions (cations and anions) which are generally present in groundwater by (A) MCCFH, (B) CPFH and (C) HECFH, respectively.

Supporting Information 11

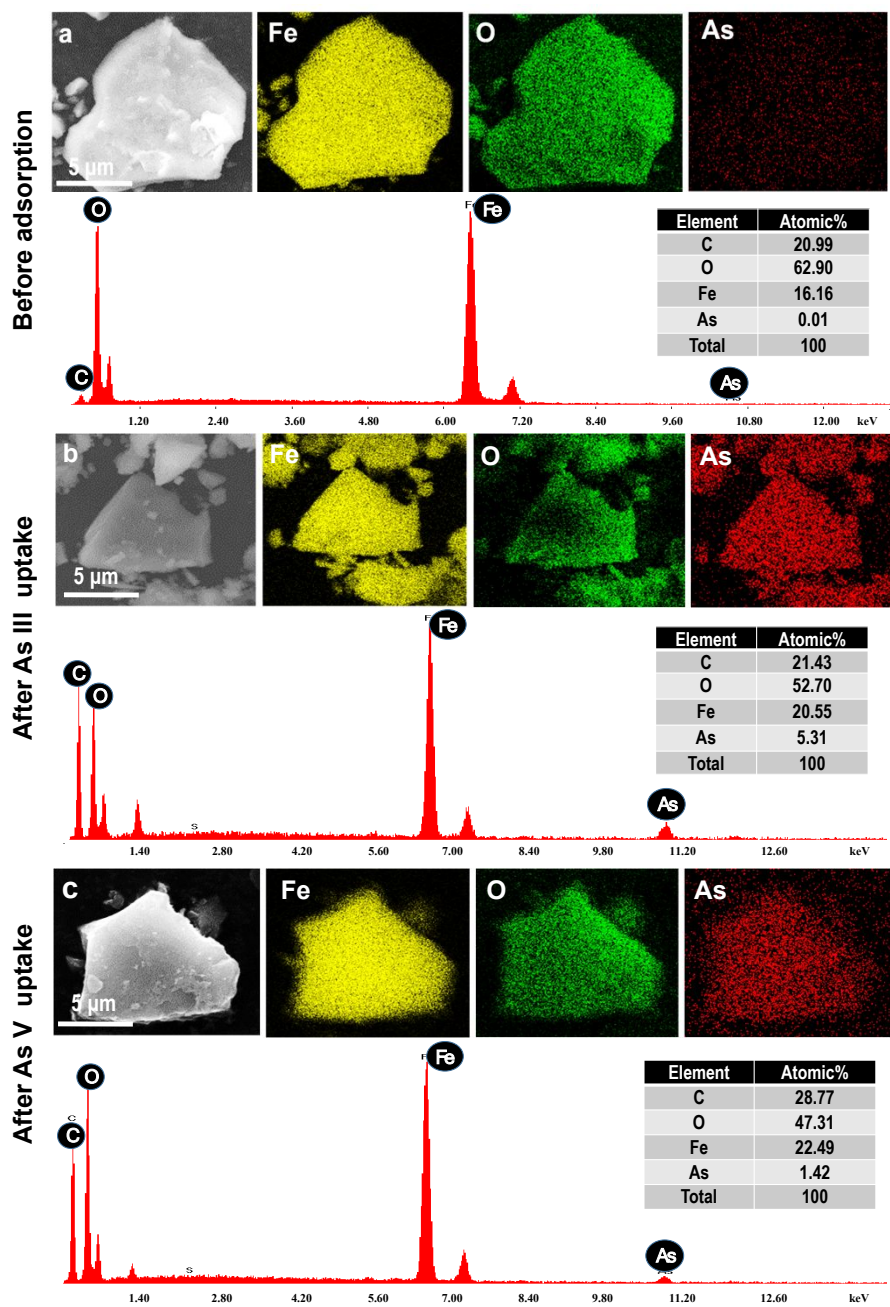


Figure S11. SEM-EDS and elemental mapping of CMCFH (a) before (b) after As(III) and (c) after As(V) adsorption.

Supporting Information 12

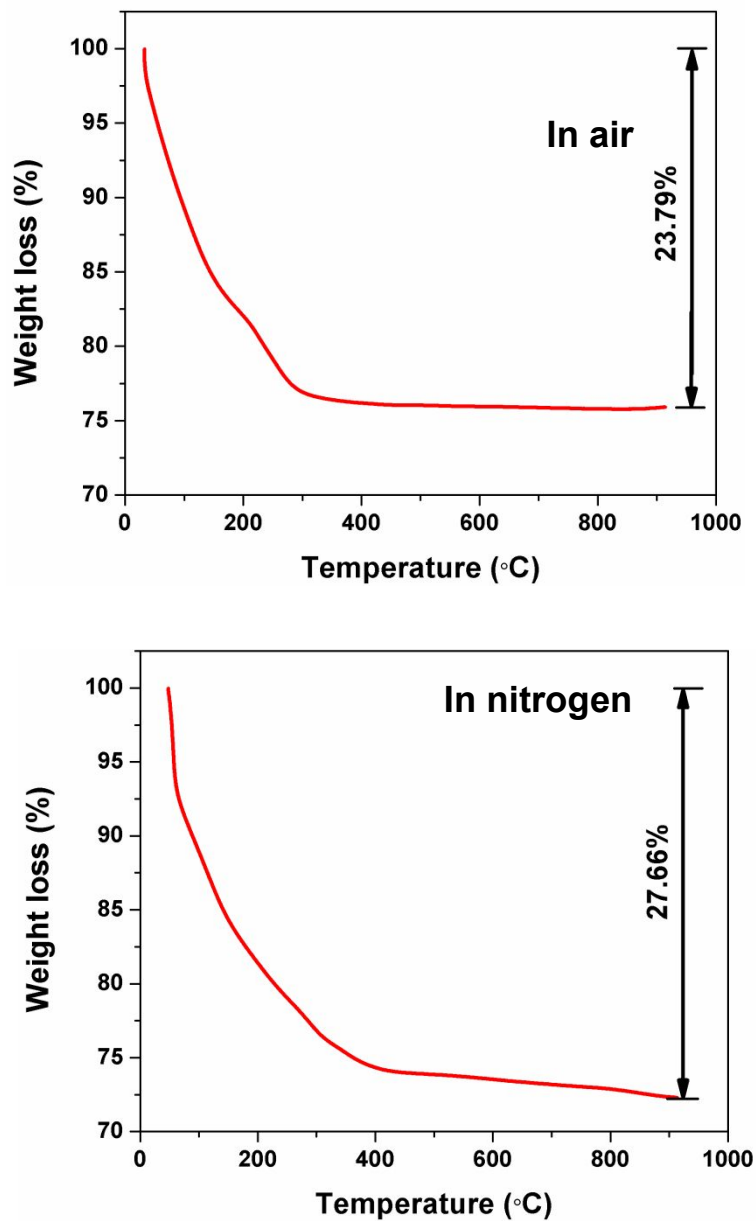


Figure S12. Thermogravimetric analysis (TGA) of CMCFH at air and nitrogen atmospheres from room temperature to 900 °C with 10 min scan rate.

Table S1.

Physicochemical characteristics of influent natural water.

Sl no.	Parameters	Value
1	Total coliforms (CFU/ml)	1-2 * 10 ³
2	pH at 25°C	7.8
3	Conductivity (µS/cm)	640.0
4	Fluoride (mg/L)	0.57
5	Chloride (mg/L)	86.34
6	Nitrate (mg/L)	1.84
7	Sulfate (mg/L)	32.41
8	Silicate (mg/L)	15.87
9	Phosphate (mg/L)	55.83
10	Sodium (mg/L)	53.74
11	Potassium (mg/L)	2.33
12	Magnesium (mg/L)	14.34
13	Calcium (mg/L)	28.72